# RF Gridded Ion Thruster Design for Laboratory Experiments

Patrick Crandall\*
University of California, Los Angeles, Los Angeles, CA, 90095, USA

Chris Cretel<sup>†</sup>

Oregon State University, Corvallis, OR, 97331, USA

Richard E. Wirz<sup>‡§</sup>
University of California, Los Angeles, Los Angeles, CA, 90095, USA
Oregon State University, Corvallis, OR, 97331, USA

RF gridded ion thrusters are simpler in construction than other gridded ion thrusters and have been shown to be more robust for air-breathing electric propulsion and alternative propellant applications than DC thrusters. ICP sources can be difficult to construct for new users who are unfamiliar with RF systems limiting adoption of RF thrusters. This work presents a basic overview of RF ion thruster concepts, ICP operating principles, antenna matching, and thruster design for new users. A lab model RF gridded ion thruster developed at the UCLA PESPL is described as a design example and preliminary performance values are presented.

## I. Introduction

RF gridded ion thrusters utilize an inductively coupled plasma (ICP) discharge to generate a plasma and a set of biased grids to accelerate the ions to high velocity generating thrust. Commercial RF ion thrusters are available in a wide range of sizes and power levels [1–3]. As the ICP discharge does not require a thermionic emitter, RF thrusters are more robust to chemically reactive propellants. In processing applications ICP discharges are commonly operated with a wide range of gasses including N2, O2, Cl, and other reactive gasses [4]. DC discharges utalizing thermionic emitters are sensitive to oxygen poisoning which rules out propellants containing oxygen and necessitates careful handling procedures to avoid contamination [5]. RF discharges are simpler in construction than similar DC thrusters requiring fewer power supplies and no hollow cathodes.

Off the shelf RF ion sources exist, but they are high cost and difficult to modify. A small lab model RF ion thruster is a useful platform for thruster experiments particularly for alternative propellant and air-breathing applications. Additionally, the high energy ion beam from the thruster can be used for investigating plasma-material interactions [6, 7]. This paper provides a brief overview of RF ion thruster operating principles and concepts and how they apply to RF ion thruster design. Design of a lab model thruster developed at the UCLA PESPL is presented along with preliminary performance results.

## II. ICP Discharge Overview

RF ion thrusters utilize an inductively coupled plasma (ICP) discharge to generate plasma in the discharge chamber. Major components of an ICP are (1) the RF antenna which is driven with an AC current, (2) the discharge chamber which confines the plasma, and (3) the plasma itself as shown in Figure 1a. The simplest instance of the ICP discharge is a cylindrical geometry. Flat "stovetop" geometries are commonly used in processing applications as they can generate plasma in a very large area. In thruster applications, cylindrical, conical, or hemispherical geometries are most common. This paper will focus on the cylindrical geometry, but the general principles are broadly applicable.

An ICP can be thought of as an air core transformer with the RF antenna as the primary winding and the plasma as a single turn secondary winding [4, 8]. Assuming a plasma already present in the discharge chamber, startup will be discussed in section II.C, current in the primary induces a current in the plasma secondary. Plasma impedance  $Z_p$  contains a real part due to collisions in the plasma and an imaginary part due to electron inertia [4, 9]. Power is

<sup>\*</sup>PhD Candidate, Mechanical and Aerospace Engineering, pcran@ucla.edu, AIAA Student Member

<sup>†</sup>PhD Student, Mechanical, Industrial and Manufacturing Engineering, cretelc@oregonstate.edu, AIAA Student Member

<sup>&</sup>lt;sup>‡</sup>Adjunct Professor, Mechanical and Aerospace Engineering, wirz@ucla.edu, AIAA Associate Fellow

<sup>§</sup> Boeing Professor, Executive Director of Aerospace Research Programs, richard.wirz@oregonstate.edu, AIAA Associate Fellow

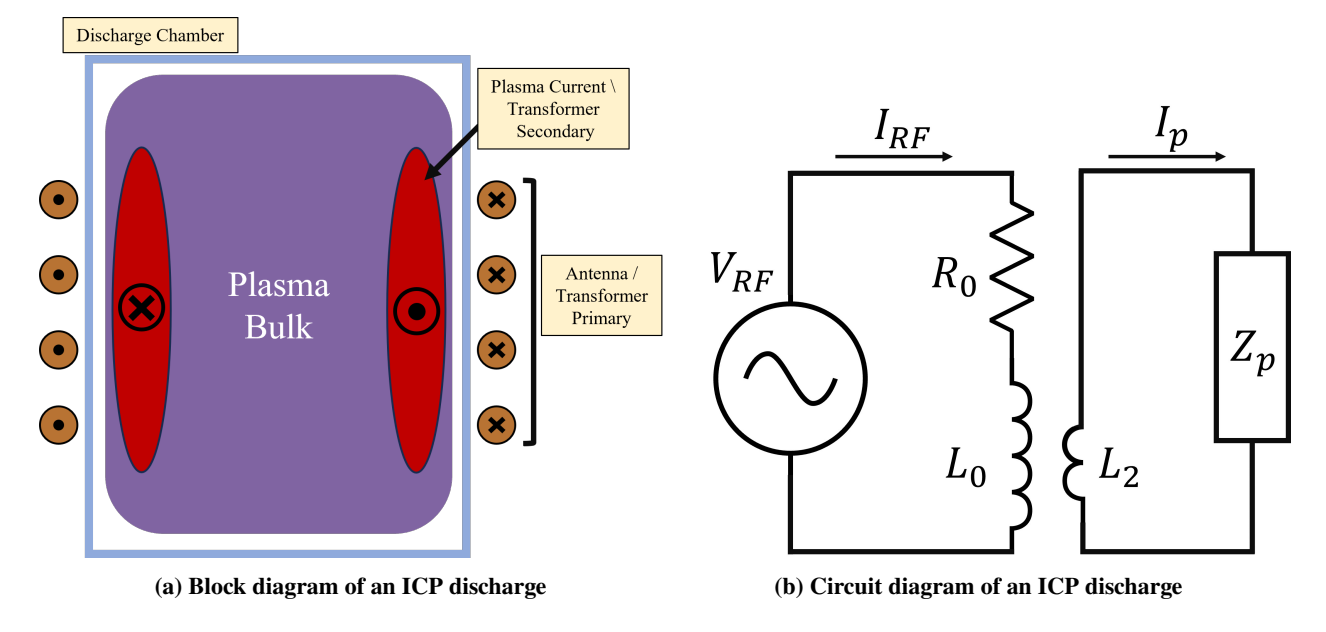


Fig. 1 Diagram of a cylindrical ICP disharge. AC current flows through four turn antenna shown in the diagram which acts as the primary winding of a transformer. Current is induced in the plasma near the antenna forming a single turn transformer secondary. The ICP discharge is represented as a transformer in a circuit diagram [8].

dissipated in the secondary due to the real part of  $Z_p$  which results in heating of the electron population to energies where ionization can be sustained, usually a few eV.

Another important power deposition mechanism for low pressure ICP discharges is stochastic heating [4, 9]. Stochastic heating is a collisionless heating method where thermal electrons are directly heated by the oscillating electric fields present at the discharge chamber walls. This effect allows for efficient ICP operation at low pressure where there are few collisions [9].

## A. Global Model

A simple global model can be used to illustrate ICP operation [4]. Steady state plasma conditions are determined by the balance of ion generation in the bulk volume and loss at the walls. Electrons in the discharge are thermally heated, so the electron energy distribution function (EEDF) can be assumed to be Maxwellian for simple models [10]. Ions are generated via collisions with high energy electrons in the tail of the EEDF. For Maxwellian plasmas, ionization and other processes such as excitation, elastic scattering, dissociation, and other processes are given in the literature as rate constants [4, 11, 12]. Rate constants are the solution to  $K(T) = \langle \sigma(v)v \rangle$  where electron velocity v is taken over the Maxwellian distribution and  $\sigma(v)$  is the collision cross section [4]. Total ion generation rate is then given as  $v_{iz} = K_{iz}n_g$  where  $n_g$  is the neutral gas density. Ions are lost to the walls where they recombine with electrons and become neutrals again. Ion loss rate is given as  $v_{loss} = u_B/d_{eff}$  where  $d_{eff}$  is the effective plasma size and  $u_B$  is the Bohm velocity [4]. Ion generation is governed by discharge chamber volume while loss is governed by surface area through  $d_{eff}$ . Thus, as device volume shrinks, ICP sources inherently become less efficient [13].

Electromagnetic waves in a plasma cannot propagate if the wave frequency is below the plasma frequency [9]. For small devices, operating frequency must be high enough such that the skin depth is less than the device radius so that maximum power is delivered to the plasma [13].

# **B.** Capacitive Coupling

Driving RF power in the coil can induce high voltages across the antenna particularly for high inductance antennas (high number of turns). In the simplest configurations, one antenna leg is grounded while the other is at an oscillating high voltage [14]. High voltages present in the antenna can capacitively couple to the plasma depositing power to the bulk plasma [9]. Capacitive coupling is less efficient than inductive coupling as high energy ion can impact the discharge chamber walls increasing losses [15]. Capacitive coupling can be reduced through the use of a Faraday shield

or through advanced match network topologies [16, 17]. A Faraday shield is a slotted metal shield placed between the antenna and the discharge chamber. The slots allow the magnetic component of the RF field to penetrate into the discharge sustaining the ICP but blocks the electric component of the RF field reducing capacitive coupling. Faraday shields are effective at reducing capacitive coupling but can add loss if poorly designed as well as increase complexity [16, 17]. Advanced match topologies rely on the use of additional capacitors in the match network to reduce voltage across the antenna coil ends as described in [17, 18].

#### C. Discharge Startup

Startup in a gridded RF ion thruster can be achieved in two ways, through the E-H mode transition, or if a neutralizer is present, reverse bias of the grids [19]. E-H mode transition is a simple way to start the discharge as no neutralizer is required, but in practice for gridded ion thrusters it may require higher RF power than normal and a gas puff. Puffing the gas initiates a capacitive plasma in the discharge chamber known as E mode which can be seen as a dim glow in the discharge chamber. Increasing RF power results in a transition to inductively coupled H mode with a corresponding sharp increase in brightness and change in impedance. After H mode is initiated, RF power can be decreased due to a hysteresis effect [19]. Starting using the E-H mode transition requires capacitive coupling, so inclusion of a Faraday shield can impede startup using this method [16].

Startup with a neutralizer already on can be performed by setting a positive bias on the accel grid drawing electrons from the neutralizer into the discharge chamber initiating the discharge. RF power and gas flow can be left at normal levels during this procedure reducing requirements on the RF generator and chamber pumping capacity. A DPDT switch can be used to easily switch accel grid polarity.

# D. Pulsed Discharges

RF discharges have the ability to operate in a pulsed mode where RF power is modulated at a frequency lower than the driving frequency. Typical pulse modulation frequency is on the order of kHz [15, 20]. Pulsed discharges are commonly used in the processing industry to control the EEDF and control reactive species generation [21]. At the beginning of a pulse cycle, RF power is driven at a high level producing a hot, dense plasma. Power is then cut off starting the afterglow period of the cycle. Electrons quickly cool reducing diffusion to the walls and slowing ion losses [4, 20].

A major challenge of implementation of pulsed discharges is maintaining a match over the whole pulse cycle [21, 22]. Plasma conditions vary over the pulse, so maintaining a match and efficient power transfer to the plasma can require advanced match techniques [23].

# **III. Antenna Matching and Other Considerations**

Antenna matching is required to effectively deliver power to the plasma. A description on how a user should approach antenna matching is provided. There are also several engineering considerations for RF ion thruster construction which can impact device operation and performance.

# A. Antenna Matching

In AC power transfer circuits, source and load impedance must be matched for effective power transfer. If there is a mismatch in the system then power is reflected from the load instead of absorbed. Load in an ICP is the combination of the antenna coil and plasma which forms a complex impedance [8]. Most commercial RF equipment has a standardized, real 50 ohm source impedance but ICPs are dynamic, complex RF loads. Therefore, insertion of an impedance matching network between the source and the load is used to transform the complex load impedance to the 50 ohm source. Several match topologies exist, but an L topology shown in Figure 2 is the most common [14]. Match topologies which utilize inductors can experience higher losses [17].

System impedance changes significantly with the presence of a plasma which requires the matching network to be robust to instantaneous changes in impedance between the on and off condition. A sharp rise in impedance can result in high voltages and breakdown of the matching network components. Plasma operating conditions also lead to changes in impedance that the matching network must be robust to.

Several ideal transformer models exist to estimate plasma impedance [8, 14]. Implementation of these models in practice can be difficult though due to nonideal effects in the system. An iterative approach is used to design the PCB

match network. The antenna is first matched with no plasma, then the impedance is measured with the plasma on and the match network is adjusted for the plasma on condition.

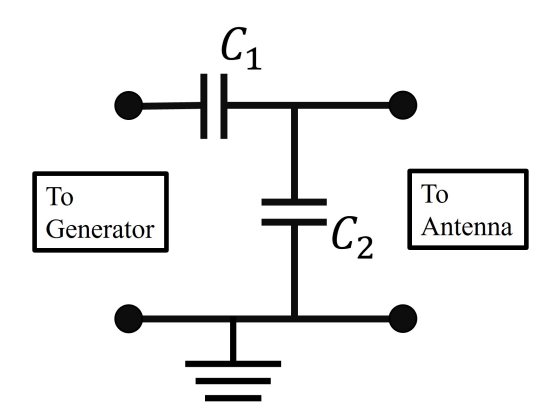


Fig. 2 Electrical diagram of an L match network [14]. In some match networks the order of the shunt and series capacitors are swapped.

The antenna with no plasma represents a complex impedance which must be matched reasonably well to the generator output to create a plasma. Antenna impedance Z = R + Xj can be measured using a vector network analyzer (VNA) connected to the antenna terminals. Coupling to the environment can be significant so VNA measurements should be taken with the antenna installed in the thruster. Complex impedances can be plotted on a Smith chart [24]. Smith charts are commonly used in impedance matching where real loads exist on the horizontal axis, inductive loads are located above the axis, and capacitive loads are located below the axis. ICP antennas are inductive loads so are located in the top portion of the Smith chart. Several programs exist to compute the required capacitor values for the match network topology shown in Figure 2 [25, 26]. The match network should be shielded from the environment in a repeatable way as coupling to metal enclosures can have a significant effect on matching. Similarly, match network capacitors should be mounted in a way which minimizes changes to the circuit for consistent matching. Capacitors should be chosen such that they are rated to the driving frequency, rated to high RF voltage, and have a flat temperature response to minimize thermal effects on the match.

Once the antenna is matched with no plasma, power can be delivered to the antenna generating a plasma. With the plasma on, the match will be poor and reflected power will be high. Load impedance with the plasma on can be measured using a directional coupler inserted on the generator side of the match network and an oscilloscope connected to the forward and reflected power outputs. The forward wave has the form  $V(t) = V^+ \sin(2\pi f t)$  with the reflected wave  $V(t) = V^- \sin(2\pi f t + \psi)$  where  $\psi$  is the phase shift between the forward and reflected waves and  $V^+$  and  $V^-$  are the wave amplitudes. The complex reflection coefficient  $\Gamma$  can be computed as: [27]

$$\Gamma = \frac{V^-}{V^+} e^{j\psi} \tag{1}$$

Impedance Z can then be computed from  $\Gamma$  using [28]:

$$Z = Z_0 \frac{1+\Gamma}{1-\Gamma} \tag{2}$$

Where  $Z_0 = 50 \Omega$ . Additionally, the standing wave ratio (SWR), s can be computed from  $\Gamma$  using  $s = \frac{1+|\Gamma|}{1-|\Gamma|}$ . SWR can be used as a measure of how well matched a load is with SWR=1 being perfectly matched.

Commercial automatic adjustable match networks are available and can adjust a set of variable capacitors to match to a broad spectrum of load impedances. These systems are useful for laboratory experiments and development where operating conditions are expected to vary widely. Adjustable match networks are generally located outside the vacuum chamber and require a high voltage feedthrough and a feed line to the source. Long feed lines can create significant losses before reaching the antenna and transform the load impedance reducing specificity of the thruster impedance and changing system response. If a current measurement on the feed line is possible, then coupler loss can be computed as described by [17]. PCB match networks with fixed capacitors may be attractive to some users as it is more similar to a flight system and minimizes losses in the coupler at the cost of reduced flexibility and more upfront development costs.

#### B. Antenna Design

In practice, the antenna coil makes a non-ideal air core transformer with the plasma which can increase loss and change the electrical response of the ICP relative to an ideal transformer model [29, 30]. A physical diagram of non-ideal effects is shown in Figure 3a.

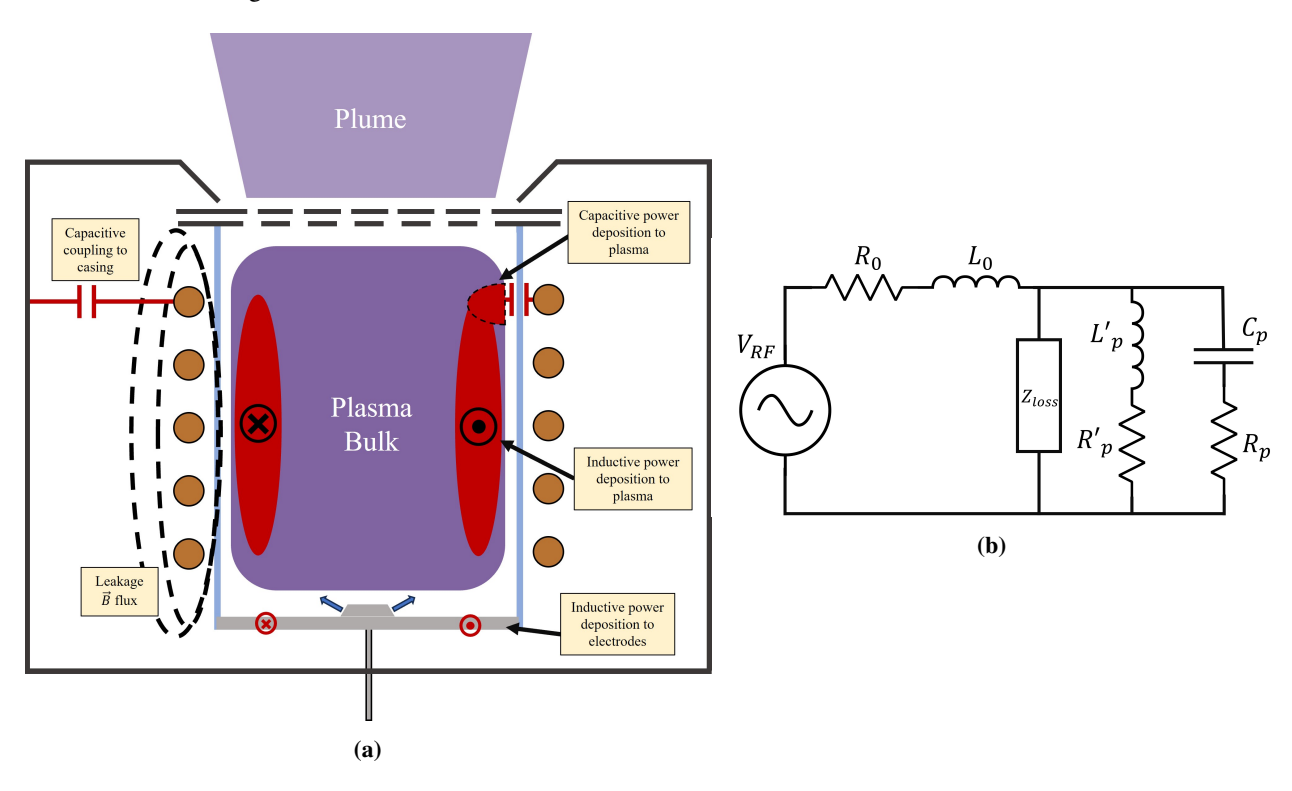


Fig. 3 Block diagram and circuit diagram of an RF gridded ion thruster showing coupling to the plasma and loss mechanisms which can have capacitive and inductive components [9, 15].

Major non-ideal transformer effects are leakage inductance, coupling to the thruster body, and the skin effect. These effects can result in weak coupling to the plasma and higher reactance increasing losses. Leakage inductance is generated magnetic field that 'leaks' between the primary and secondary and does not contribute to current generation in the secondary [31]. In an ICP this is determined by the discharge chamber wall thickness. A thin discharge chamber increases inductive power transfer, but also increases capacitive coupling, a less efficient mechanism [15, 17]. On the opposite side of the coil to the load, the antenna can couple to the thruster casing, grids, and other metal parts near the coil. Coupling to the casing determines the minimum device size where smaller devices will have more coupling to the coil and higher loss. The skin effect causes increased coil heating by increasing wire resistance in the antenna. At high frequency current tends to travel on the surface of conductors instead of through the bulk of the material as in DC circuits reducing the effective size of the conductor.

## C. RF Safety

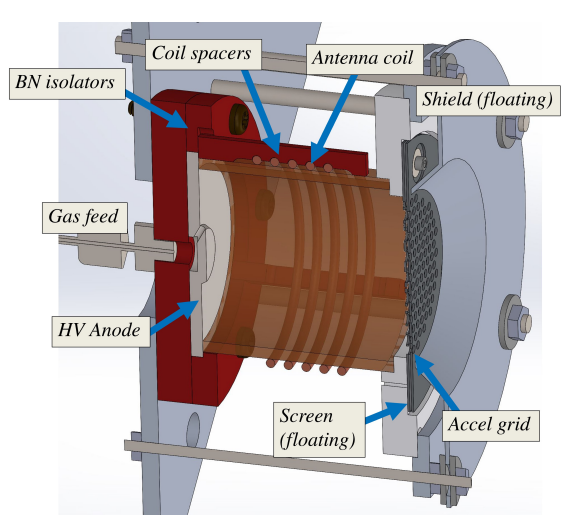
RF systems can emit harmful levels of non-ionizing radiation if not properly shielded. OSHA recommends a voluntary maximum exposure of  $10 \text{ mW/cm}^2$  while FCC regulations limit exposure to  $900/f \text{ mW/cm}^2$  where f is the frequency in MHz [32, 33]. The American Radio Relay League provides information on safe operation of RF devices [34]. Care should always be taken to shield users from RF radiation particularly with high-power devices.

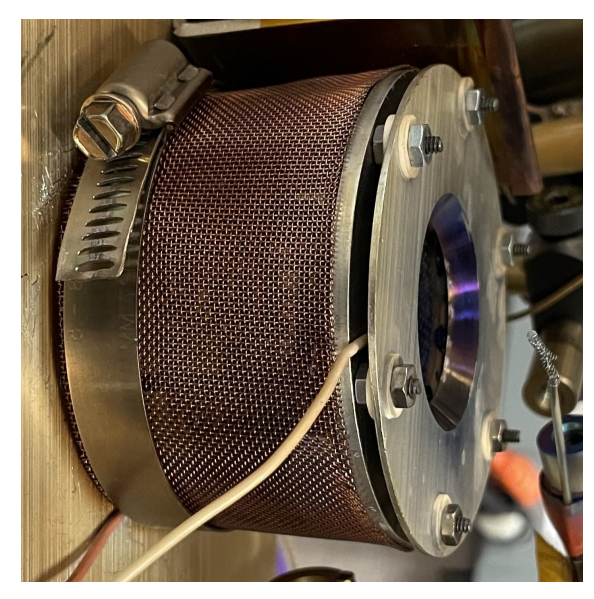
## **IV. PESPL RF Ion Thruster**

A 3 cm RF gridded ion thruster was developed at UCLA with the goal of studying ABEP gridded ion thruster performance. Thruster design was influenced by commercial miniature RF gridded ion thruster designs such as BIT-3, NPT30-I2, and RIT-4, as well as taking heritage from the 3cm MiXI DC discharge thruster [13, 35–37].

#### A. Thruster Hardware

A CAD model of the thruster with major components labeled is shown as Figure 4a. Unique features of the thruster include a dedicated anode and a floating screen grid [38]. A dedicated anode was chosen to provide additional electrical contact to the plasma, simplify gas distribution, and provide a replaceable electrode for materials studies.





(a) Design model of the thruster

(b) Assembled thruster

Fig. 4 CAD model of the thruster showing major components and photo of the thruster in the vacuum chamber. The thruster in the photo is connected to an adjustable match network outside the vacuum chamber via a cable.

The grid face is 3 cm in diameter with ion optics similar to the NSTAR gridded ion thruster [39]. Precise grid spacing is achieved using metal shim washers placed in oversized cutouts in the screen grid to avoid electrical contact between the grids. The floating shield located downstream of the grids blocks the exposed screen grid mounts from the neutralizer so there is no direct current path from the neutralizer to the anode through the discharge and discourages neutralizer coupling to facility ground [40]. A Macor grid mount holds the grid assembly and interfaces with the discharge chamber. A 35 mm long quartz tube with 2 mm wall thickness is used as the discharge chamber. Additionally, the clear discharge chamber allows easy access for spectrographic diagnostics. At the rear of the discharge to the grids is the high voltage (HV) anode which also serves to distribute gas in the discharge chamber. The discharge chamber tube is held in place between the grid assembly and the anode by tension rods. Angled holes drilled in the anode divert propellant gas away from the grid face reducing neutral losses [13]. The gas feed connection is left floating to eliminate any current paths through the gas feed. Boron nitride is used for the base construction material shown in red due to its machinability and high temperature tolerance. Antenna spacers were used in some iterations to maintain the antenna shape and coil spacing. A 5-turn antenna coil is wrapped around the discharge chamber. The antenna is made of 14 AWG magnet wire. A filament neutralizer made from 0.005" diameter tungsten wire is mounted downstream of the thruster.

#### **B. Electrical System**

A circuit diagram of the UCLA thruster electrical system is given as Figure 5 showing all power supplies.

Three DC power supplies are used in the UCLA thruster, the beam supply, the accel grid supply, and the neutralizer supply. All three supplies supplies are connected to the common rail which is allowed to float relative to facility ground through a resistor. A TVS diode in parallel with the resistor acts as a safety device keeping common from charging to high voltage if the neutralizer fails. Common is allowed to float to ensure the beam supply draws current from the neutralizer and not ground. Beam voltage  $V_b$  is connected to the anode biasing the plasma discharge to the beam voltage which is generally > 1 kV. The accel grid is biased negative with respect to common to block electrons from the neutralizer from reaching the discharge. For the UCLA thruster,  $V_{accel}$  is set between -150 to -300 V with higher voltages allowing higher beam current at the cost of increased charge exchange erosion. The filament neutralizer is

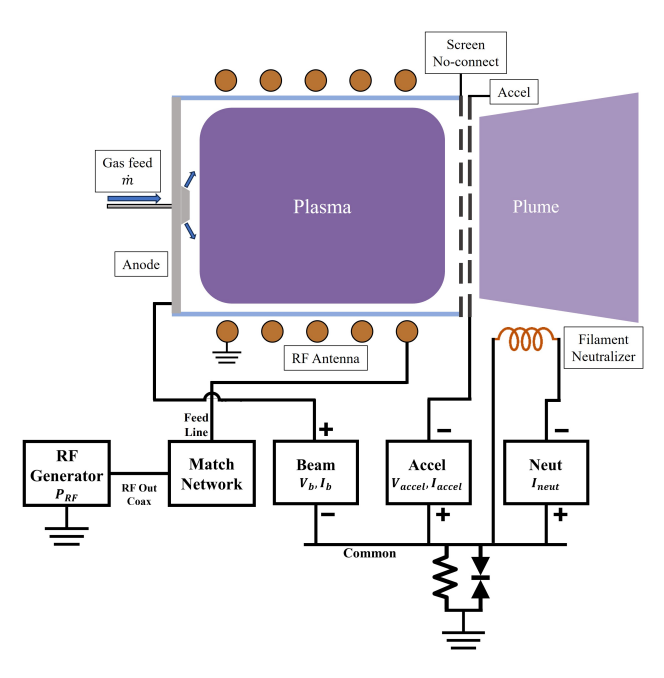


Fig. 5 Block Diagram of the thruster showing connections with all power supplies. The resistor in the diagram has a value of 50 kOhms, and it allows the common rail to float relative to ground. A parallel TVS diode trips at 100 V keeping common from floating to dangerous voltages if the neutralizer fails.

positioned near the plume and is driven with current from the neutralizer (neut) supply heating the filament.  $I_{neut}$  is increased to the point where the filament reaches sufficient temperature to thermionically emit electrons.

The RF generator produces RF power for the antenna and is connected to the match network through a coaxial cable. An industrial standard for ICPs is 13.56 MHz making generators at this frequency common, but lower frequencies are generally more efficient [13]. A match network matches the load to the 50 Ohm generator output using either fixed or adjustable capacitors. The UCLA thruster can be operated using either an Advanced Energy Cesar 13.56 MHz plasma generator paired with an Advanced Energy VM600A automatic adjustable match network or an Electronics & Innovation 1020L 10 kHz – 5MHz broadband power amplifier with a fixed match network shown in Figure 7. For the adjustable match network configuration, the match network is located outside the vacuum chamber, so a feed line is required to deliver power to the thruster antenna. A LMR400 coax cable was used as the feed line to the vacuum feedthrough and RG400 coaxial cable was used inside the vacuum chamber. Initial tests resulted in overvoltaging at the TNC vacuum feedthrough. This issue was resolved by increasing the length of the vacuum side feed line reducing the voltage at the RF feedthrough but resulting in higher feed line loss. The RG400 cable shielding was spliced, and a Pearson current monitor was placed along the line to monitor current and estimate coupler loss. Coupler loss is measured using equations:  $P_p = P_t - P_c$  and  $P_c = \left(\frac{I_c}{I_{c0}}\right) P_{c0}$  where  $P_p$  is power delivered to the plasma,  $P_t$  is power transmitted from the RF generator,  $P_c$  is power lost in the coupler,  $I_c$  and  $I_{c0}$  are current with the plasma on and off respectively, and  $P_{c0}$  is power delivered to the coupler with the plasma off [17].

For the fixed match network configuration, the match network is connected directly to the antenna eliminating the feed line and reducing loss. RF power is fed via LMR100 SMA coaxial cables from the power amplifier into the vacuum chamber to the match network. In this configuration, the match network is downstream of the vacuum feedthrough, so there are not high voltages at the vacuum feedthrough as in the adjustable match case. Significant power loss occurs in the cabling between the power amplifier and the match network, so cable loss must be accounted for. A directional coupler can be placed at the match network input to directly measure forward power, reflected power, and load impedance with the plasma on. During testing it was found that the power amplifier had different gain for cases with the plasma on and off due to load mismatch with the plasma off. During plasma ignition, the sharp impedance change resulted in higher power output from the generator frequently resulting in a fault. Mitigation of this issue is ongoing while testing continues with the Cesar RF generator and adjustable match network.

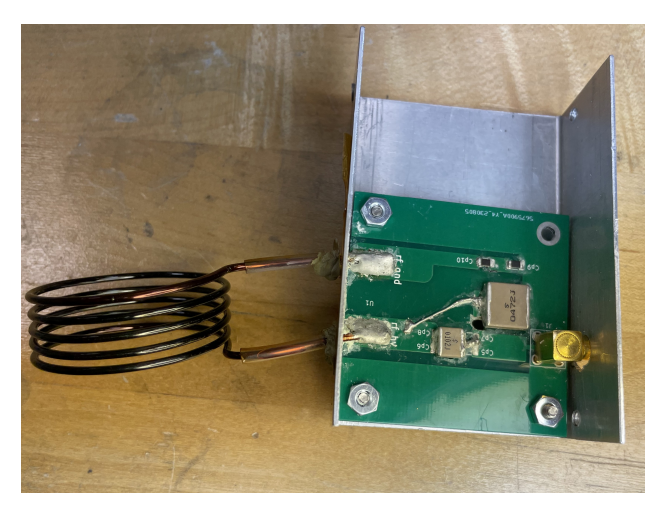


Fig. 6 Photo of the fixed capacitor match network with the cover removed and antenna. RF power is delivered from the generator via a 50 Ohm SMA connector. Slots for a termination capacitor are included on the PCB but shorted in this photo [18].

## C. Preliminary Performance Values

Preliminary thruster testing was performed with xenon and argon propellants using the adjustable match network. One setpoint with each propellant is shown in Table 1. Neglecting doubly charged species and plume divergence, thrust T is computed as  $T = \sqrt{\frac{2M}{e}}I_b\sqrt{V_b}$  where M is the ion mass,  $I_b$  is beam current, e is the fundamental charge, and  $V_b$  is the beam voltage.  $I_b$  and  $V_b$  are measured from the anode power supply. From thrust, specific impulse  $I_{sp} = \frac{T}{\dot{m}g}$  and thrust-to-power  $T/P = \frac{T}{P_{RF} + V_b I_b}$  can be computed where  $\dot{m}$  is mass flow rate, g = 9.81 m/s<sup>2</sup>, and  $P_{RF}$  is the RF power delivered to the thruster.

Propellant	Xe	Ar
Anode voltage [V]	2000	1200
Anode current [mA]	67	70
Accel voltage [V]	-300	-300
Propellant flow rate [sccm]	2.5	6
Delivered RF power [W]	69	81
Discharge loss [eV/ion]	1028	1160
Electrical efficiency	0.66	0.51
Mass efficiency	0.37	0.16
Total efficiency	0.25	0.08
Thrust [mN]	4.9	2.21
$I_{sp}$ [s]	2065	1261
T/P [mN/kW]	24.4	13.4

Table 1 Preliminary performance results for the thruster running on xenon and argon using NSTAR style grids.

Mass utilization efficiency is relatively low reducing total efficiency. Lower transparency grids should be used to mitigate this issue. The thruster discharge showed more stability at higher RF power resulting in high beam current. Simulations in charge exchange 2D predict a maximum  $I_b$  before grid impingement of 70 mA, so grid impingement is likely due to beam non-uniformity. Low transparency grids may improve discharge stability at low power. Grid sputtering onto the discharge chamber was observed during testing decreasing RF power delivered to the plasma over time



Fig. 7 Photo of the thruster operating on argon propellant with a shielded filament neutralizer. The version shown included capacitors on the grids to reduce RF pickup, but were removed in later versions.

# **D.** Alternative Configurations

The PESPL thruster can be easily reconfigured to act as a large RF cathode by replacing the grid face with a single orifice as described in [41]. In cathode configuration, the anode electrode in the thruster now acts as an ion collector collecting positive charge from the discharge with negative charges passing through the orifice [42, 43]. Thus, hardware changes are minimized between the thruster and cathode configurations.

## V. Conclusion

RF gridded ion thrusters are robust devices useful for laboratory experiments for new EP devices and investigation in areas such as PMI and plasma-based manufacturing. For EP, RF ion sources are particularly attractive for alternative propellants and emerging applications such as ABEP. A review of principles of RF gridded ion thruster design is provided to increase accessibility of these thrusters to new users. These principles were applied to create a low-cost lab model thruster at the UCLA PESPL for ABEP and alternative propellant experiments. The lab thruster allows for spectroscopy access and is easily repaired and reconfigured. Preliminary performance results are provided for xenon and argon propellants. Continuing efforts are underway to improve thruster stability and performance and to evaluate thruster performance over a larger operating space. Results from these future efforts will be reported in forthcoming publications.

## Acknowledgments

The authors would like to thank Dr. Patrick Pribyl for his helpful advice on ICP matching and construction. This work was supported by DOE Award DE-AR0001378, "AMPERE: Advanced Materials for Plasma Exposed Robust Electrodes".

# References

- [1] Ariane Group, "Electric Ion Space Propulsion Systems and Thrusters,", 2023. URL https://www.space-propulsion.com/spacecraft-propulsion/propulsion-systems/electric-propulsion/index.html.
- [2] Busek Company, "RF Ion Thrusters,", 2023. URL https://www.busek.com/rf-ion-thrusters.
- [3] ThrustMe, "The NPT30-I2,", 2023. URL https://www.thrustme.fr/products/npt30-i2.
- [4] Lieberman, M. A., and Lichtenberg, A. J., "Principles of plasma discharges and materials processing," *MRS Bulletin*, Vol. 30, No. 12, 1994, pp. 899–901.

- [5] Polk, J., "The Effect of Reactive Gases on Hollow Cathode Operation," 42nd AIAA/ASME/SAE/ASEE Joint Propulsion Conference & Exhibit, 2006, p. 5153.
- [6] Sabiston, G., and Wirz, R. E., "Thrust Densification of Space Electric Propulsion Systems via Volumetrically Complex Materials," AIAA SCITECH 2024 Forum, 2024.
- [7] Li, G. Z., and Wirz, R. E., "Persistent sputtering yield reduction in plasma-infused foams," *Physical Review Letters*, Vol. 126, No. 3, 2021, p. 035001.
- [8] Godyak, V., Piejak, R., and Alexandrovich, B., "A simple analysis of an inductive RF discharge," *Plasma Sources Sci. Technol*, Vol. 1, 1992, p. 36.
- [9] Chabert, P., Tsankov, T. V., and Czarnetzki, U., "Foundations of capacitive and inductive radio-frequency discharges," *Plasma Sources Science and Technology*, Vol. 30, No. 2, 2021, p. 024001.
- [10] Godyak, V. A., Piejak, R., and Alexandrovich, B., "Electron energy distribution function measurements and plasma parameters in inductively coupled argon plasma," *Plasma Sources Science and Technology*, Vol. 11, No. 4, 2002, p. 525.
- [11] Gudmundsson, J. T., "Notes on the Electron Excitation Rate Coefficients for the Argon and Oxygen Discharge," 2002.
- [12] Gudmundsson, J. T., "Electron Excitation Rate Coefficients for the Nitrogen Discharge," 2005.
- [13] Loeb, H. W., and Schartner, K., "Development Of RIT-Microtrhusters," 55 th International Astronautical Congress, 2004.
- [14] Chen, F. F., "Capacitor tuning circuits for inductive loads," UCLA Report, 1992.
- [15] Piskin, T., Qian, Y., Pribyl, P., Gekelman, W., and Kushner, M. J., "E-H transitions in Ar/O2 and Ar/Cl2 inductively coupled plasmas: Antenna geometry and operating conditions," *Journal of Applied Physics*, Vol. 133, No. 17, 2023.
- [16] Godyak, V., Piejak, R., and Alexandrovich, B., "Experimental setup and electrical characteristics of an inductively coupled plasma," *Journal of applied physics*, Vol. 85, No. 2, 1999, pp. 703–712.
- [17] Godyak, V., and Alexandrovich, B., "Power measurements and coupler optimization in inductive discharges," *Review of Scientific Instruments*, Vol. 88, No. 8, 2017.
- [18] Suzuki, K., Konishi, K., Nakamura, K., and Sugai, H., "Effects of capacitance termination of the internal antenna in inductively coupled plasma," *Plasma Sources Science and Technology*, Vol. 9, No. 2, 2000, p. 199.
- [19] Kortshagen, U., Gibson, N., and Lawler, J., "On the E-H mode transition in RF inductive discharges," *Journal of Physics D: Applied Physics*, Vol. 29, No. 5, 1996, p. 1224.
- [20] Ashida, S., Lee, C., and Lieberman, M. A., "Spatially averaged (global) model of time modulated high density argon plasmas," *Journal of Vacuum Science & Technology A*, Vol. 13, No. 5, 1995, pp. 2498–2507. https://doi.org/10.1116/1.579494.
- [21] Banna, S., Agarwal, A., Cunge, G., Darnon, M., Pargon, E., and Joubert, O., "Pulsed high-density plasmas for advanced dry etching processes," *Journal of Vacuum Science & Technology A*, Vol. 30, No. 4, 2012.
- [22] Qu, C., Lanham, S. J., Shannon, S. C., Nam, S. K., and Kushner, M. J., "Power matching to pulsed inductively coupled plasmas," *Journal of Applied Physics*, Vol. 127, No. 13, 2020.
- [23] Advanced Energy, "Navigator® II Digital Matching Networks,", 2023. URL https://www.advancedenergy.com/getmedia/251b89ab-67a3-4a39-a8fc-f45c48dbacf4/en-ppg-navigator-digital-matching-networks-data-sheet.pdf.
- [24] Caspers, F., "RF engineering basic concepts: the Smith chart," arXiv preprint arXiv:1201.4068, 2012.
- [25] Fritz Dellsperger, "Smith V4.1,", 2023. URL https://www.fritz.dellsperger.net/smith.html.
- [26] Mathworks, "Matching Network Designer,", 2023. URL https://www.mathworks.com/help/rf/ref/matchingnetworkdesigner-app.html.
- [27] Çankaya University, "The complex reflection coefficient,", 2023. URL https://ece358.cankaya.edu.tr/uploads/files/Ece358Exp5. pdf.
- [28] Mathworks, "gamma2z,", 2023. URL https://www.mathworks.com/help/rf/ref/gamma2z.html.

- [29] Meziani, T., Colpo, P., and Rossi, F., "Electrical description of a magnetic pole enhanced inductively coupled plasma source: Refinement of the transformer model by reverse electromagnetic modeling," *Journal of applied physics*, Vol. 99, No. 3, 2006.
- [30] Godyak, V., and Chung, C.-W., "Distributed ferromagnetic inductively coupled plasma as an alternative plasma processing tool," *Japanese journal of applied physics*, Vol. 45, No. 10S, 2006, p. 8035.
- [31] McLyman, C. W. T., Transformer and inductor design handbook, CRC press, 2004.
- [32] Occupational Safety and Health Administration, "Radiofrequency and Microwave Radiation,", 2023. URL https://www.osha.gov/radiofrequency-and-microwave-radiation/standards.
- [33] Federal Communications Commission, "Section 1.1310 Radiofrequency radiation exposure limits.", 2023. URL https://www.govinfo.gov/content/pkg/CFR-2011-title47-vol1/xml/CFR-2011-title47-vol1-sec1-1310.xml.
- [34] American Radio Relay League, "Section 1.1310 RF Exposure,", 2023. URL https://www.arrl.org/rf-exposure.
- [35] Tsay, M., Hohman, K., and Olson, L., "Micro RF ion engine for small satellite applications," 2009.
- [36] Rafalskyi, D., Martínez, J. M., Habl, L., Zorzoli Rossi, E., Proynov, P., Boré, A., Baret, T., Poyet, A., Lafleur, T., Dudin, S., et al., "In-orbit demonstration of an iodine electric propulsion system," *Nature*, Vol. 599, No. 7885, 2021, pp. 411–415.
- [37] Samples, S. A., and Wirz, R. E., "Development of the MiXI Thruster with the ARCH Discharge," *Plasma Research Express*, Vol. 2, No. 2, 2020, p. 025008.
- [38] Tsay, M. M.-T., "Numerical modelling of a radio-frequency micro ion thruster," Ph.D. thesis, Massachusetts Institute of Technology, 2006.
- [39] Wang, J., Polk, J., Brophy, J., and Katz, I., "Three-dimensional particle simulations of NSTAR ion optics," 27th International Electric Propulsion Conference, Pasadena, CA, 2001.
- [40] Patterson, M. J., and Mohajeri, K., "Neutralizer optimization," International Electric Propulsion Conference, 1991.
- [41] Leiter, H., Altman, C., Lauer, D., Rath, M., Becker, F., Feili, D., and Gonzalez de Amo, J., "A Nouvelle Neutralization Concept for RIT-µX Miniaturized Radio Frequency Ion Thruster Systems," 36th International Electric Propulsion Conference, Vienna, Austria, IEPC-2019-806. https://electricrocket.org/2019/806.pdf, 2019.
- [42] Watanabe, H., Ichimura, M., and Takegahara, H., "Performance of a Hall thruster operating with a radio frequency plasma cathode," 52nd AIAA/SAE/ASEE Joint Propulsion Conference, 2016, p. 4947.
- [43] Watanabe, H., Hatakeyama, T., Irie, M., Okutsu, A., Tsukahara, T., Aoyagi, J., and Takegahara, H., "Study on Radio frequency Cathode for Ion engines," *Transactions of the Japan Society for Aeronautical and Space Sciences, Space Technology Japan*, Vol. 7, No. ists26, 2009, pp. Pb\_53–Pb\_58.